Thomas-Ehrman effect in a three-body model: The ^{16}Ne case

L. V. Grigorenko,[1,2,3] T. A. Golubkova,[4] and M. V. Zhukov[5]
[1]*Flerov Laboratory of Nuclear Reactions, JINR, RU-141980 Dubna, Russia*
[2]*National Research Nuclear University MEPhI, Kashirskoye shosse 31, RU-115409 Moscow, Russia*
[3]*National Research Center "Kurchatov Institute," Kurchatov sq. 1, RU-123182 Moscow, Russia*
[4]*Advanced Educational and Scientific Center, Moscow State University, Kremenchugskaya 11, RU-121357 Moscow, Russia*
[5]*Fundamental Physics, Chalmers University of Technology, S-41296 Göteborg, Sweden*
(Received 3 November 2014; revised manuscript received 14 January 2015; published 25 February 2015)

The dynamic mechanism of the Thomas-Ehrman shift in three-cluster systems is studied by using the example of ^{16}Ne and ^{16}C isobaric mirror partners. We predict configuration mixings for 0^+ and 2^+ states in ^{16}Ne and ^{16}C. Large isospin symmetry breaking on the level of wave function component weights is demonstrated for these states and discussed as a three-body mechanism of the Thomas-Ehrman shift. It is shown that the description of the Coulomb displacement energies requires consistency among three parameters: the ^{16}Ne decay energy E_T, the ^{15}F ground-state energy E_r, and the configuration mixing parameters for the ^{16}Ne and ^{16}C 0^+ and 2^+ states. Based on this analysis we infer the ^{15}F $1/2^+$ ground-state energy to be $E_r = 1.39$–1.42 MeV.

DOI: 10.1103/PhysRevC.91.024325 PACS number(s): 21.60.Gx, 21.10.Dr, 21.10.Sf, 21.45.−v

I. INTRODUCTION

This paper probes whether the Thomas-Ehrman shift (TES) can be used to gain more insight into the low-lying ^{16}Ne spectrum and the properties of the even s-d shell nuclei beyond the proton drip line in general.

The TES is an effect of isobaric symmetry violation, which was initially introduced for single-particle states of sd-shell nuclei in Refs. [1,2]. In such nuclei the $l = 0$ and $l = 2$ orbitals are quite close to degeneracy. However, these orbitals have different radial extent and their Coulomb displacement energies (CDEs) are quite different. Therefore the relative positions of the $l = 0$ and $l = 2$ orbitals in isobaric partner states are strongly affected by the presence (absence) of the Coulomb interaction. These differences provide, e.g., a simple way for l identification. Later, studies of the TES effect have also been extended to nuclei with even number of "valence" nucleons, with the goal, e.g., understanding of configuration mixing.

There is no solid definition of the TES, so, let us recall those typically used in the literature. One possibility is a kind of "theoretical" definition in which one considers the difference between the experimental CDE and the one expected from isobaric symmetry,

$$\Delta_J = \Delta_{\rm Coul}({\rm calc}) - \Delta_{\rm Coul}({\rm pert}), \qquad (1)$$

for a state with total spin J. $\Delta_{\rm Coul}$(calc) is the CDE obtained by solving the Schrödinger equation (SE) on both the proton and neutron sides of the isobar, while $\Delta_{\rm Coul}$(pert) is the perturbative CDE obtained by solving the SE on the *neutron* side of the isobar and then using the obtained wave function (WF) to calculate the CDE on the proton side perturbatively by assuming complete isobaric symmetry:

$$\Delta_{\rm Coul}({\rm pert}) = \langle \Psi_n | V_{\rm Coul} | \Psi_n \rangle.$$

Such a definition was used, e.g., in Refs. [3–5].

A phenomenological analog of the value (1) was analyzed in Ref. [6]. This work compared experimental masses $M_{\rm exp}$ with masses $M_{\rm cg}$ provided by the charge-symmetric mass relationship

$$\Delta_J = M_{\rm exp} - M_{\rm cg}.$$

Such an analysis relies only on the information about masses and excitation energies and it can be performed in an unambiguous and statistically significant way. A systematic increase in the value of the TES was demonstrated in [6] for systems beyond the proton drip line with increasing proton (or two-proton) Q values.

The other possibility is to use a pure "phenomenological" definition which relies only on the experimental relative shifts of the energy levels with different J values in proton-rich and neutron-rich mirror systems:

$$\Delta_{J_2 J_1} = [E(J_2) - E(J_1)]_{\rm prot} - [E(J_2) - E(J_1)]_{\rm neut}. \qquad (2)$$

An analysis of this definition of this TES compared with the one of Eq. (1) can be found in Ref. [3].

The interpretation of the TES for systems with one valence nucleon is very simple as we have already mentioned. The energies of single-particle orbitals with $l = 2$ can be found around the values defined by the perturbative Coulomb displacement, and Δ_J for these should be relatively small. The energies of single-particle orbitals with $l = 0$ are shifted to considerably lower energies than perturbative values, and Δ_J for these should be large. As a result, the distance between levels (and sometimes even the level ordering) is changing, inducing a sizable $\Delta_{J_2 J_1}$.

The situation is more complicated for systems with two valence nucleons. A simple estimate illustrating that is as follows. For the sd-shell WFs of the 0^+ and 2^+ states can schematically be approximated as

$$\Psi_0 = \alpha_0 [s^2]_0 + \beta_0 [d^2]_0, \quad \Psi_2 = \alpha_2 [sd]_2 + \beta_2 [d^2]_2. \quad (3)$$

If we think in terms of the independent particle model and consider that a typical value of the TES associated with an s-wave nucleon is Δ, and with the d-wave nucleon being zero, then, e.g., for $\alpha_0 = 1$ and $\alpha_2 = 0$ we can expect $\Delta_{20} = 2\Delta$

while for $\alpha_0 = 0$ and $\alpha_2 = 1$ we can expect $\Delta_{20} = -\Delta$. Thus, in principle, the important structure information is encoded in the $\Delta_{J_2 J_1}$ value, but it still cannot be extracted without considerable theoretical work, in contrast with the one-valence-nucleon case.

The existence of a specific realization of the TES, characterized as a "three-body mechanism" of the TES, was demonstrated in Ref. [4]. ^{12}O, ^{16}Ne, and their isobaric mirror partners ^{12}Be and ^{16}C were considered in a three-body core + $N + N$ model. It was shown that in such systems not only a conventional (or "static") TES exists, which is connected with the different radial extent of the $[s^2]$ and $[d^2]$ configurations. Also there arises a specific TES of a three-body nature (a "dynamic" TES) for which the relative weights of $[s^2]$ and $[d^2]$ configurations appeared to be strongly different in the neutron-rich and proton-rich mirror partners. A strong increase (tens of percent) was predicted for the weight of the $[s^2]$ configuration on the proton side of the isobar caused by the presence of the core-p Coulomb interaction.

Recently, ^{16}Ne was studied in three experiments using neutron knockout from a ^{17}Ne beam [7–9], providing data with better statistics and quality than in the previous works. This inspired us to revisit the issue and consider the TES effect in ^{16}Ne and ^{16}C also in the broader context including the first excited 2^+ states. We demonstrate in this work that the TES can be used as a very precise tool to check the consistency of three-body core + $N + N$ and two-body core + N state properties.

II. THEORETICAL MODEL

The theoretical model of this work is the same as was previously used for the discrete spectrum [10] and continuum [11] studies in a three-body approach. It was applied to ^{16}Ne and its isobaric mirror partner ^{16}C in Refs. [4,9]. Here we describe the model mainly to clarify details connected with our accurate TES treatment.

For studies of ^{16}C, the discrete spectrum states are solutions of a homogeneous three-body Schrödinger equation

$$(\hat{H}_3 - E_T)\Psi_3(\rho,\Omega_5) = 0, \tag{4}$$

where the energy E_T is calculated with respect to the core + $N + N$ threshold. For studies of the ^{16}Ne continuum spectrum an inhomogeneous three-body Schrödinger equation

$$(\hat{H}_3 - E_T)\Psi_3^{(+)}(\rho,\Omega_5) = \Phi_{\mathbf{q}}^{(J)}(\rho,\Omega_5) \tag{5}$$

is solved for each J different energies E_T searching for the resonance peak position. The source function $\Phi_{\mathbf{q}}^{(0)}$ for the ^{16}Ne ground state (g.s.) was approximated by assuming a sudden removal of a neutron from the ^{15}O core of ^{17}Ne,

$$\Phi_{\mathbf{q}}^{(0)} = v_0 \int d^3 r_n \, e^{i\mathbf{q}\mathbf{r}_n} \langle \Psi_{^{14}\mathrm{O}} | \Psi_{^{17}\mathrm{Ne}} \rangle, \tag{6}$$

where $\mathbf{r}_n$ is the radius vector of the removed neutron. The ^{17}Ne g.s. WF $\Psi_{^{17}\mathrm{Ne}}$ was obtained in [12] in a three-body $^{15}\mathrm{O} + p + p$ model, and different aspects of nuclear dynamics for this system were investigated in [13]. The WF of the removed neutron was constructed in the cluster $^{14}\mathrm{O} + n$ model approximation for ^{15}O in such a way that the neutron separation energy and experimental matter radius of ^{15}O are reproduced. The details of the whole procedure can be found in Ref. [14]. The value of the rms radius, 3.05 fm, for the $^{14}\mathrm{O} + n$ channel WF was found by using rms matter radii of 2.44(4) fm (^{15}O) and 2.40(3) fm (^{14}O) from Ref. [15].

For the 2^+ excitations of ^{16}Ne we do not have some simple dynamically motivated model and $\Phi_{\mathbf{q}}^{(2)}$ was provided by additionally acting on the valence protons of the ^{17}Ne g.s. WF by the quadrupole operator:

$$\Phi_{\mathbf{q}}^{(2)} = v_2 \int d^3 r_n e^{i\mathbf{q}\mathbf{r}_n} \langle \Psi_{^{14}\mathrm{O}} | \sum_{i=1,2} r_i^2 \, Y_{2m_i}(\hat{r}_i) | \Psi_{^{17}\mathrm{Ne}} \rangle. \tag{7}$$

The sudden removal approximation is not intended for absolute cross-section calculations; therefore the "source strength" coefficients v_J are arbitrary values providing the source functions the correct dimension [energy/length$^{5/2}$].

It should be noted that the approaches to discrete spectrum and continuum states is explicitly different in Eqs. (4) and (5). There are two things to emphasize: (i) The formulation provided by Eq. (5) is a simplistic but reasonable approximation for the neutron knockout reaction mechanism used to populate ^{16}Ne states in the recent experimental studies [7–9]. Therefore, the differences in the approaches (4) and (5) is physically motivated. (ii) The practical difference between results provided by Eqs. (4) and (5) vanishes in the limit of the widths tending to zero for continuum states. For 0^+ and 2^+ states of ^{16}Ne considered in this work (which are very narrow), the effect of a particular choice of the sources $\Phi_{\mathbf{q}}^{(J)}$ on the energies of the calculated resonances is less than some units of keV, which is much less than the other effects considered here.

The three-body WF Ψ_3 depends on a set of hyperspherical variables: the hyperradius ρ and the five-dimensional hyperangle Ω_5. The hyperspherical decomposition of the discrete spectrum WF is

$$\Psi_3(\rho,\Omega_5) = \rho^{-5/2} \sum_{K\gamma} \chi_{K\gamma}(\rho)\mathcal{J}_{K\gamma}(\Omega_5). \tag{8}$$

The value K is the hypermoment (the principal quantum number of the hyperspherical method) while the "multiindex" $\gamma = \{L,S,l_x,l_y\}$ stands for the complete set of quantum numbers for the specific three-body WF component: total orbital momentum L, total spin S, and orbital angular momenta l_x and l_y for the Jacobi subsystems. The boundary conditions for the discrete spectrum partial hyperspherical functions $\chi_{K\gamma}$ are expressed in terms of Bessel functions K as

$$\begin{aligned} \chi_{K\gamma}(\rho) &\overset{\rho\to\infty}{\sim} \sqrt{2\varkappa\rho/\pi}\, K_{K+2}(\varkappa\rho) \\ &\sim \exp[-\varkappa\rho]\left(1 + \frac{4(K+2)^2 - 1}{8\varkappa\rho} + \cdots\right), \end{aligned} \tag{9}$$

where $\varkappa = \sqrt{2ME_T}$, and M is the average mass of the nucleon in the considered system. At large distances (tens of Fermi) this is essentially an exponential decrease. For example, for the $K = 0$ component of the ^{16}C g.s. WF, the largest nonconstant term in the long-range decomposition in Eq. (9) becomes small compared to unity (less than 0.1) at ρ values larger than 36 fm.

The decomposition of the continuum WF $\Psi_3^{(+)}$ is analogous to that of Eq. (8). The boundary conditions for the partial continuum functions $\chi_{K\gamma}^{(+)}$ at extreme remote asymptotic hyperradius (where the long-range Coulomb terms vanish because of some form of physical screening) should be provided by diverging waves:

$$\chi_{K\gamma}^{(+)}(\rho) \overset{\rho\to\infty}{\sim} \exp[i\varkappa\rho]. \tag{10}$$

However, for realistic distances of actual calculations (e.g., $\rho \sim 1000$ fm) we use complicated approximate boundary conditions for the three-body Coulomb problem obtained by diagonalization of the Coulomb potential terms in the hyperspherical representation on the finite hyperspherical basis [11].

The three-body Hamiltonian consists of the kinetic term, three pairwise interactions, and the phenomenological potential V_3 depending only on the hyperradius ρ:

$$\hat{H}_3 = \hat{T} + V_{\text{core-}N_1} + V_{\text{core-}N_2} + V_{N_1\text{-}N_2} + V_3(\rho). \tag{11}$$

The V_3 term *technically* aims at fine correction of the state energies when we need to adjust them exactly to experimental values, and it *physically* accounts for many-body effects which are beyond the three-body dynamics [11]. In this work we use for this term the Woods-Saxon form factor

$$V_3(\rho) = V_3^{(J)} \big/ \{1 + \exp[(\rho - \rho_0)/a_\rho]\}, \tag{12}$$

with the radius $\rho_0 = 6$ fm and diffuseness $a_\rho = 0.6$ fm. The V_3 potential depth parameter $V_3^{(J)}$ is adjusted individually for each total spin J (see Table I, for example).

For the $^{14}Z + N$ channel ($Z = 9,6$) we use the potentials very similar to those from Refs. [4,9], but with minor variations connected with the procedure of the TES treatment discussed in the next paragraph. These are Woods-Saxon potentials with derivative (ls) term

$$V_{\text{core-}N_i} = V_c^{(l)} \frac{1}{1 + f(r)} + (\mathbf{l}\cdot\mathbf{s})\, V_{ls}^{(l)} \frac{b}{ra} \frac{f(r)}{[1 + f(r)]^2},$$
$$f(r) = \exp\left[\left(r - r_0^{(l)}\right)/a\right],$$

where $b = 2.015\,32$ fm^2. The components of the potentials are l dependent: they are adjusted individually for the quantum states with different angular momenta. The following parameters are used for s, p, and d orbitals: $a = 0.53$ fm, $V_c^{(1)} = -12$ MeV, $V_{ls}^{(1)} = 11$ MeV, $r_0^{(1)} = 2.89$ fm, $V_{ls}^{(2)} = -11.12$ MeV, and $r_0^{(2)} = 3$ fm. The other central component parameters for s and d waves are provided in Table I. There is also an additional repulsive component in the s wave with Woods-Saxon form factor with repulsion 144 MeV, width 1.7 fm, and diffuseness 0.53 fm. This is required to simulate the effect of the occupied deep s orbital in the ^{14}Z core cluster in our three-body model.

In this work we employ for the nucleon-nucleon channel the quasirealistic potential from Ref. [16] including central, spin-orbit, tensor, and parity-splitting terms.

The Coulomb potential of a homogeneously charged sphere was used in this work with sphere radius adjusted to reproduce the specific charge radius. We also estimated the influence of the charge distribution on the effect of using Gaussian and Fermi-type form factors. The impact of such a modification on energies is on the level of 10–15 keV, which is much smaller than the scale of energy uncertainty connected with uncertainty of the charge radius itself.

TABLE I. Potential sets in the core + N channel adjusted for $r_{\text{ch}}(^{14}\text{O}) = 2.7$ fm. Radii are in fm, energies in MeV, and probabilities in percent. The position E_r of the two-body resonance is defined here by the phase shift equal to $\pi/2$. The energy of the first excited state of ^{15}F is $E_r(5/2^+) = 2.8$ MeV.

	P1	P2	P3	P4	P5
$E_r(1/2^+)$	1.147	1.287	1.467	1.287	1.287
$r_0^{(0)}$	3.5	3.1	2.7	3.1	3.1
$V_c^{(0)}$	−34.085	−47.45	−67.9	−47.45	0
$V_c^{(2)}$	−49.587	−49.587	−49.587	0	−49.587
$V_3^{(0)}$	0.255	0.647	1.051	−2.461	−1.918
Δ_{Coul}(pert)	7.017	7.130	7.301	6.517	7.561
			^{16}C(0^+)		
$W(s^2)$	44.2	47.8	51.4	93.5	0.82
$W(p^2)$	0.88	0.86	0.83	5.47	9.01
$W(d^2)$	46.5	43.1	39.9	0.71	89.8
			^{16}Ne(0^+)		
E_T	1.136	1.303	1.514	0.821	1.972
Γ (keV)	0.323	1.09	3.67	0.003	0.313
$W(s^2)$	71.7	70.2	69.0	95.4	1.16
$W(p^2)$	5.88	5.84	5.98	3.67	9.59
$W(d^2)$	22.2	23.4	24.6	0.62	88.8
$V_3^{(2)}$	0.355	0.72	1.09		−2.697
Δ_{Coul}(pert)	6.927	7.062	7.229		7.436
			^{16}C(2^+)		
$W(p^2)$	4.67	4.79	4.9		2.50
$W(d^2)$	15.9	14.6	13.3		94.8
$W(sd)$	78.1	78.4	80.6		2.07
			^{16}Ne(2^+)		
E_T	2.941	3.074	3.232		3.585
Γ (keV)	40.6	45.2	51.4		5.25
$W(p^2)$	3.72	3.89	4.06		3.08
$W(d^2)$	7.72	7.81	7.87		91.6
$W(sd)$	87.2	86.9	86.7		4.43

In the large-basis calculations we treat part of the basis adiabatically. The potential matrix of the large size $K_{\max}$ is reduced to the size K_{FR} by a procedure which is called Feschbach reduction. This is essentially an adiabatic approximation (see, e.g., Ref. [17] for details). A reduced potential matrix of size K_{FR} is used to solve the system of hyperspherical coupled channel equations. A $K_{\max}$ equal to 110 and 70 is used for the 0^+ and 2^+ states correspondingly, while the K_{FR} values are 24 and 18. Such basis sizes are sufficient for computational convergence of such complicated decay observables as widths and momentum distributions [9,17]. They are more than sufficient for full convergence of the energy calculations.

III. COMPUTATION PROCEDURE FOR THE TES

There are two uncertain ingredients in the three-body model computation of the TES in the ^{16}Ne-^{16}C mirror partner pair:

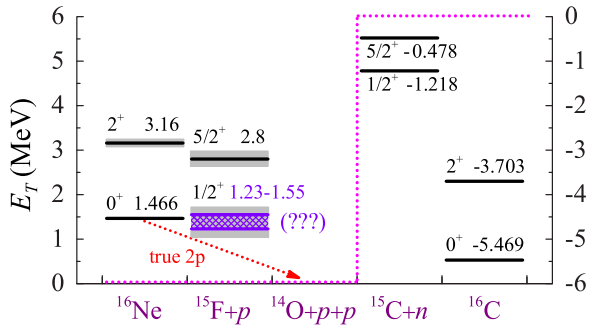

FIG. 1. (Color online) Energy level schemes for ^{16}Ne (from [9]), ^{15}F (left axis), and ^{16}C and ^{15}C (right axis). The true $2p$ decay path for the ^{16}Ne g.s. is indicated by the red dotted arrow. The hatched area indicates the experimental uncertainty of the ^{15}F g.s. position.

(i) the charge radius $r_{\rm ch}$ of ^{14}O, which is experimentally unknown (see, e.g., Ref. [18]), and (ii) the $1/2^+$ ground-state energy E_r of ^{15}F, which strongly affects the results of the calculations, but on which there exists an experimental controversy (see, e.g. Ref. [19]). The level schemes for ^{16}Ne-^{16}C and ^{15}F-^{15}C isobaric mirror partner pairs are shown in Fig. 1.

Preparing the potential sets we fix the positions of $1/2^+$ and $5/2^+$ states of $^{15}\mathrm{C} = {}^{14}\mathrm{C} + n$ to be exactly experimental values by using potentials of somewhat different radii r_0 in the corresponding partial wave. Then we switch to ^{15}F, getting different resonant state positions $E_r(J^\pi)$ depending on the potential radius and also on $r_{\rm ch}$ of ^{14}O. Based on the trend of known charge radii for oxygen isotopes [18] the charge radii of ^{14}O around 2.7 fm are used. The d-wave potential radius is thus fixed based on the well-known position of the $5/2^+$ state in ^{15}F. The $1/2^+$ state position in ^{15}F is varied depending on specific r_0 and $r_{\rm ch}$. For relatively broad states, to which the ^{15}F g.s. belongs, there is always some uncertainty in the definition of the state position. In this work we always imply that E_r is the energy at which the phase shift passes $\pi/2$.

With the obtained potential sets we run three-body model calculations for ^{16}C. The phenomenological three-body potential parameters $V_3^{(J)}$ are adjusted to provide exact experimental energies of 0^+ and 2^+ states of ^{16}C, $E_T(0^+) = -5.469$ MeV and $E_T(2^+) = -3.703$ MeV. With $V_3^{(J)}$ parameters adjusted in this way we then perform the calculations for ^{16}Ne. The results for several potential sets (P1, P2, and P3), giving different ^{15}F g.s. positions, are provided in Table I. In the table we show only the calculation inputs and results for the charge radius $r_{\rm ch}(^{14}\mathrm{O}) = 2.7$ fm since the values obtained with different charge radii differ insignificantly.

It is seen in Table I that for realistic potentials P1–P3 the values of $V_3^{(J)}$ are quite small, typically below 1 MeV. They are also quite similar for both 0^+ and 2^+ states. This indicates that the three-body picture of the inert ^{14}O-^{14}C core plus two nucleons is an adequate approximation to the structure of these low-lying states in ^{16}Ne-^{16}C.

To test the sensitivity of the TES to the structure, we varied the s/d ratio of the WF by the following procedure: We increased the $[s^2]$ content of the WF by multiplying the d-wave potential depth parameter $V_c^{(2)}$ by a factor smaller than unity, and vice versa to increase the $[d^2]$ content of the WF we multiply the s-wave potential depth parameter $V_c^{(0)}$ by a factor smaller than unity. Two limiting cases of such potential sets (P4 and P5) are illustrated in Table I. The P4 results for the 2^+ state are missing there as it is not possible to construct a low-lying 2^+ state only on the s-wave orbitals.

IV. CALCULATION RESULTS

A. Charge radius dependence

Figure 2 shows that calculations with potentials providing different positions of the ^{15}F g.s. produce very different positions of both 0^+ and 2^+ states of ^{16}Ne. For variation of $E_r(1/2^+)$ within the range 1.23–1.56 MeV, "allowed" by uncertainty in existing experimental data, the three-body resonance energies E_T variation in ^{16}Ne is 250–300 keV. In contrast, the predicted curves for different ^{14}O charge radii practically overlap (the deviations being less than 15 keV). Thus the influence of the specific value of the unknown charge radius of ^{14}O on the physically motivated calculation results (those with fixed ^{15}F g.s. position) is practically negligible and will not significantly affect the conclusions of this work concerning the TES.

B. Three-body TES mechanism

In Ref. [4] it was demonstrated that there are two major sources of TES in the 0^+ ground states of even sd-shell nuclei present in the three-body core + N + N approximation: (i) conventional "static" TES connected with larger spatial extent of the s-wave orbitals compared to the d-wave orbitals and (ii) a "dynamic" three-body TES mechanism leading to a relative increase of the $[s^2]_0$ configuration weight compared to that of the $[d^2]_0$ configuration.

Both effects are illustrated by Fig. 3, which shows the radial density dependence for two dominant components of ^{16}Ne and ^{16}C g.s. WFs. The $K = 0$ component weight is very close to that of the $[s^2]_0$ configuration and the selected

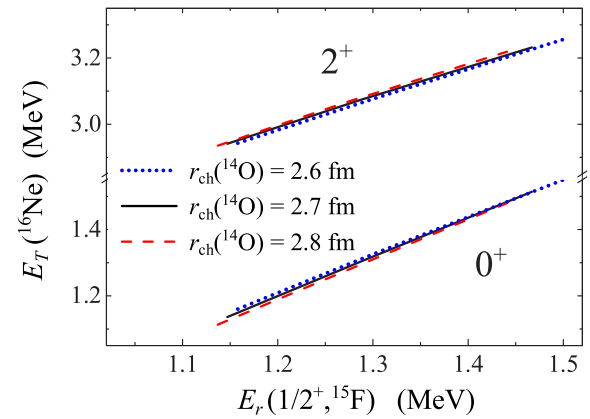

FIG. 2. (Color online) Dependence of the ^{16}Ne 0^+ and 2^+ state energies on the position of the g.s. $1/2^+$ resonance in ^{15}F. Calculations for potential sets with different charge radii of ^{14}O are shown to be nearly overlapping.

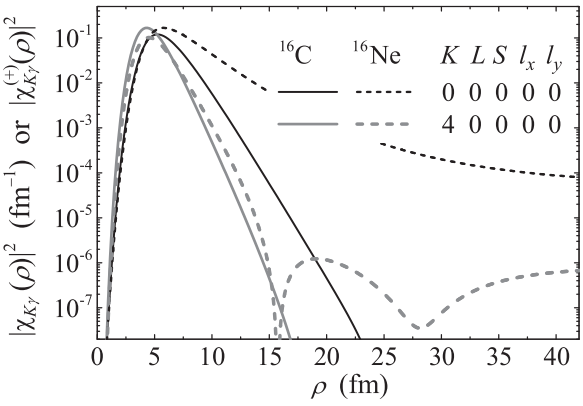

FIG. 3. Radial density dependence of two major components of three-body WFs for the ground 0^+ states of ^{16}Ne and ^{16}C, using potential set P2. The ^{16}C WF is normalized to unity, and the ^{16}Ne WF is normalized arbitrarily for ease of viewing.

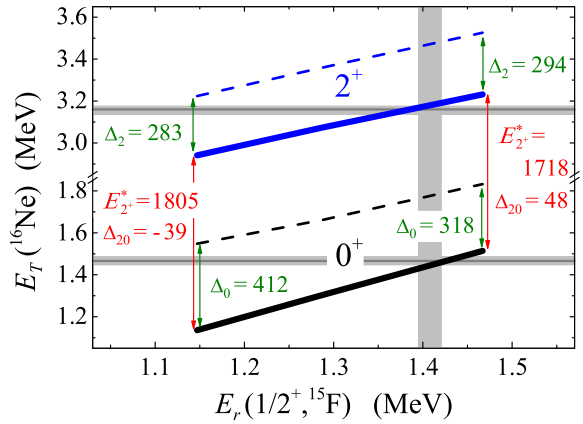

FIG. 4. (Color online) Dependence of the 0^+ and 2^+ state energies in ^{16}Ne on the position of the g.s. $1/2^+$ resonance in ^{15}F for dynamical (solid lines) and perturbative (dashed lines) calculations. The thickness of theoretical curves corresponds to ∼15 keV uncertainty connected to the choice of the charge distribution form factor. Horizontal gray lines and shaded areas show the experimental E_T values for 0^+ and 2^+ states from Ref. [9] with their uncertainties. The vertical shaded area indicates the range of E_r where a consistency between the theory and the experiment is achieved. The 2^+ state excitation energies $E^*_{2^+}$ and the TES values corresponding to different definitions provided by Eqs. (1) and (2) are indicated in the plot.

$K = 4$ component corresponds well to the $[d^2]_0$ configuration. The densities of ^{16}C WF components at large hyperradii demonstrate behavior which is close to an exponential decrease. The densities of ^{16}Ne WF components tend to become constant at large hyperradii, which corresponds to an $\sim \exp[i\varkappa\rho]$ asymptotic of the WF $\Psi_3^{(+)}$. The radial extent of the $[d^2]_0$ component in ^{16}Ne is a bit larger but close to that in ^{16}C. In contrast, the $[s^2]_0$ component is drastically broader in ^{16}Ne. Also the weight of the $[s^2]_0$ component in ^{16}Ne is evidently larger than in ^{16}C, while the weight of the $[d^2]_0$ component is smaller.

The relative scale of "static" and "dynamic" TES effects can be understood from Table I. The calculations with potential sets P4 and P5 provide limiting cases (practically pure s wave or pure d wave) of the ^{16}Ne-^{16}C structure which are very "robust" and are not altered by the Coulomb interaction. Thus the TES value Δ_0 for the 0^+ state associated solely with the radial size increase of orbitals from ^{16}C to ^{16}Ne is ∼230 keV for pure $[s^2]$ and ∼120 keV for pure $[d^2]$ configurations. In contrast, the predicted TES for the realistic structure of ^{16}Ne-^{16}C also includes the dynamic effect of structure modification and thus varies between ∼300 and ∼ 400 keV. Therefore we can estimate the scale of the "dynamic" contribution as 45%–60% of the whole TES.

C. The ^{15}F ground-state issue

The calculated positions of the 0^+ and 2^+ states in ^{16}Ne as functions of the ^{15}F g.s. energy are shown in Fig. 4. This figure also compares dynamical and perturbative results.

"Theoretical" TES values Δ_J are always large in our calculations for both the 0^+ state (varying between ∼300 and ∼400 keV) and the 2^+ state (stable at ∼300 keV) in ^{16}Ne. In contrast, the "phenomenological" TES value $\Delta_{J_1 J_2}$ is small and even changes sign, being sensitive to the particular value of E_r in ^{15}F. The latter result can probably be qualitatively understood as follows: If we look in Table I we see that the weight $W(s^2)$ varies between 44% and 51% for 0^+ in ^{16}C, while $W(sd)$ is more stable around 79% for 2^+. Thus, there are two s-wave nucleons in 0^+, which are subject to strong TES, but the weight of this configuration is mainly under 50%. There is only one s-wave nucleon in the $[sd]$ configuration of 2^+; however, the weight of this configuration is about twice as large in 2^+ than $W(s^2)$ in 0^+. So, for such structures of 0^+ and 2^+ states, the TES modifications of CDE are about equal.

Figure 4 shows that simultaneous consistent theoretical description for both 0^+ and 2^+ resonances [9] is achieved at $E_r = 1.39$–1.42 MeV. For theoretical calculations in [9] we used a potential giving $E_r = 1.45$ MeV. We see now that this value is a bit too large considering the TES results of this work. However, slight modification of this parameter on such a level does not lead to any modification of conclusions of Ref. [9] related to basic theory.

The current experimental situation for ^{15}F g.s. is quite uncertain (see, e.g., the discussion in Ref. [19]). Table II shows the results of the four most recent experiments. All of them were for the resonance scattering of ^{14}O on protons, so coinciding results are expected. This is practically true for

TABLE II. Properties of the ^{15}F $1/2^+$ g.s. and the first excited $5/2^+$ state obtained in the recent experiments on resonance scattering of ^{14}O on protons and in the theoretical analysis of this work. All values are in MeV.

Ref.	$E_r(1/2^+)$	$\Gamma(1/2^+)$	$E_r(5/2^+)$	$\Gamma(5/2^+)$
[20]	1.51(15)	1.2	2.853(45)	0.34
[21]	$1.45^{+0.16}_{-0.1}$	0.7	2.795(45)	0.325(60)
[22]	1.23(5)	0.67(17)	2.81(2)	0.30(6)
[23]	1.31(1)	0.85(15)	2.78(1)	0.31(1)
This work	1.405(15)			

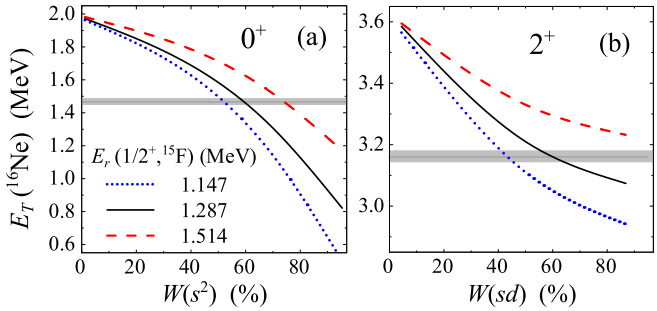

FIG. 5. (Color online) (a) Dependence of the ^{16}Ne 0^+ state energy on the weight of the $[s^2]$ WF component and (b) dependence of the ^{16}Ne 2^+ state energy on the weight of the $[sd]$ WF component. Horizontal gray lines and shaded areas show the experimental values for 0^+ and 2^+ states from Ref. [9] with corresponding uncertainty.

the first excited state, but not for the ground state of ^{15}F. Given the high uncertainty of experimental situation the consistency check found in this work may provide now the most reliable information on the ^{15}F g.s. energy.

The positions of the 0^+ and 2^+ states in ^{16}Ne as functions of the internal structure are shown in Fig. 5. Such curves allow us to fix the configuration mixing values in the case when the decay energy E_T is known. However, in our calculations we demonstrate that this can be made differently, depending on the particular $1/2^+$ resonance energy in ^{15}F. Figure 5 shows that for the 0^+ state consistency with the experiment [9] is achieved for a broad range (from 50% to 75%) of possible configuration mixing $W(s^2)$ values, depending on the specific g.s. energy E_r of ^{15}F. Consistency with experiment [9] for the 2^+ state can be achieved for from 40% to 100% of possible $W(sd)$ values. However, for the 2^+ state the situation is more restrictive as for $E_r \gtrsim 1.45$ MeV consistency of the TES with the experimental energy cannot be achieved at all.

If we fix the three-body state energies E_T to be exactly experimental [9] we can get the region on the planes $\{W(s^2), E_r\}$ or $\{W(sd), E_r\}$ where mutually consistent values of W and E_r are located (see Fig. 6). The meaning of these

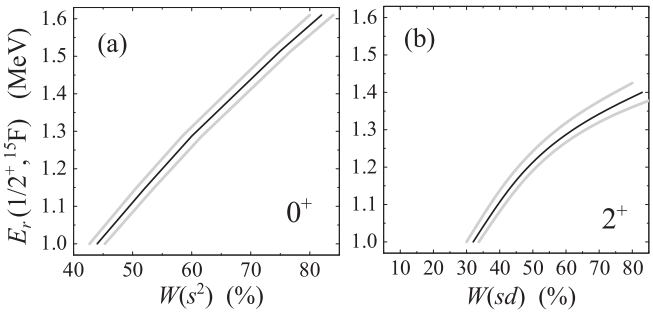

FIG. 6. Two-dimensional $\{W, E_r\}$ plots for ^{16}Ne for (a) the $[s^2]$ WF component weight for 0^+, $W(s^2)$, and (b) the $[sd]$ 2^+ WF component weight $W(sd)$ vs the energy of the ^{15}F g.s. under the restriction of reproducing exactly the experimental energies of the ^{16}Ne g.s., $E_T = 1.466(20)$ MeV, and 2^+ state, $E_T = 3.16(2)$ MeV [9]. Gray curves correspond to the limits defined by the experimental uncertainty of the above energies.

plots is that precisely fixing the g.s. properties of ^{15}F fixes the structure of the valence configurations for both 0^+ and 2^+ states of ^{16}Ne simultaneously. We note again that while for the 0^+ state consistency in principle can be achieved for a broad range of E_r, which is much broader than existing experimental uncertainty, for the 2^+ state this kind of plot becomes quite restrictive, limiting a possible E_r value to be less than 1.43–1.45 MeV. Thus we see that simultaneous studies of the TES for 0^+ and 2^+ states imposes stringent limitations on possible properties of the core $+ N + N$ systems and its core $+ N$ subsystems.

The value $E_r = 1.39$–1.42 MeV deduced in this work for the ^{15}F g.s. appears very precise. Still there are two inherent uncertainties: (i) the experimental uncertainty of E_T and (ii) the theoretical uncertainties of the three-body $^{14}\mathrm{O} + p + p$ model for ^{16}Ne. Theoretical uncertainties which go beyond the three-body formulation for ^{16}Ne should further increase this uncertainty. Thus, an admixture of configurations like $^{14}\mathrm{O}^* + p + p$ should lead to a CDE increase (with these configurations being more compact than the main one) and thus shifts the consistency range to somewhat lower E_r values. Considering the good description of energies of ^{16}Ne-^{16}C in our model we do not expect a large admixture of such configurations and making simple estimates we can suggest a 15–30 keV decrease of the lower boundary of E_r for a 10%–20% admixture of configurations with an excited 2^+ state of the ^{14}O core. This would extend the boundaries for the "TES-based" ^{15}F g.s. position to $E_r = 1.36$–1.42 MeV.

D. Structure of ^{16}Ne 0^+ and 2^+ states

The variation of the ^{15}F g.s. energy in the range allowed by the current experimental uncertainty produces some variations in the structure of ^{16}Ne and ^{16}C states calculated in the three-body model. These were found to be the largest for the ^{16}C ground state, where $W(s^2)$ varies on the level of 6%–8%. For its isobaric mirror partner, this uncertainty is significantly reduced. In ^{16}Ne the typical level of structure variation is 2%–3% and can be regarded as insignificant. We can guess that for ^{16}Ne the peripheral dynamics, associated with the long-range Coulomb interaction rather than with the short-range nuclear dynamics, is more important and this leads to the relative stabilization of the calculated results for the 0^+ state in ^{16}Ne.

For the 2^+ state the predictions are much more stable than for the 0^+ state and also follow the trend discussed above: There is ~2.5% variation of $W(sd)$ in the ^{16}C WF and just ~0.5% variation in the ^{16}Ne WF. Both values can be regarded as very small and the predicted structure as stable.

Quite a paradoxical output of our studies is that the presence of the Coulomb interaction drastically increases the reliability of theoretical predictions for a class of systems such as ^{16}Ne-^{16}C on the proton side of the isobar.

E. Widths of the ^{16}Ne 0^+ and 2^+ states

The results of width calculations (see Table I) are shown in Fig. 7. They are accompanied with the calculated results from Ref. [4]. The latter work was one of the first of our works on

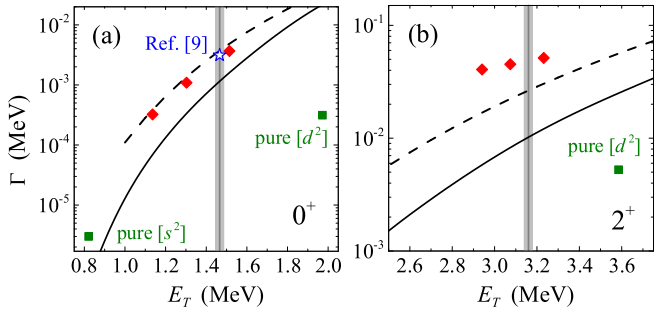

FIG. 7. (Color online) The widths of the ^{16}Ne 0^+ and 2^+ states. Solid and dashed curves are three-body calculations and diproton model estimates from Ref. [4]. Red diamonds are results of calculations with different E_r values from Table I. Green squares show the results of calculations with limiting cases of nuclear structure: pure $[s^2]$ or pure $[d^2]$. The blue star shows the 0^+ result from Ref. [9]. Vertical gray lines and dashed areas correspond to experimental energies from Ref. [9] and their uncertainties.

the topic and the results provided there suffered from some technical issues, which were later overcome [11].

It can be seen that our new results for the 0^+ state [red diamonds in Fig. 7(a)] are around a factor of 4 larger than those from Ref. [4] (solid curves in Fig. 7). However, they follow the trend provided by the old prediction very well. So, the difference is a pure convergence issue, connected to the small-basis calculations a decade ago.

A different situation is found for the 2^+ state widths. The newly calculated results differ from the old ones even more and here they clearly follow a different energy trend. Here we have to conclude that the three-body width increase connected with the decrease of the $1/2^+$ state energy in the ^{15}F subsystem "outweighs" the three-body width decrease connected with the corresponding shift to lower E_T energies.

The width results for the pure $[d^2]$ configuration (green squares in Fig. 7) are always more than an order of the magnitude lower than the value expected by continuing the trend for realistic structure calculations or calculations with $[s^2]$ dominance. This is an indication of the uncertainty range for the two-proton decay widths, which, in principle, can be associated with unknown nuclear structure.

V. EXPERIMENTAL DATA ON ^{16}Ne 0^+ AND 2^+ STATES

Figure 4 demonstrated the consistency of our theoretical TES values with the most recent experimental data [9] on ^{16}Ne0^+ and 2^+ states. The situation is, however, different for the other data.

The available experimental data on ^{16}Ne 0^+ and 2^+ states are listed in Table III. The first thing which should be noted is that already the ground-state data are still quite uncertain, spanning from 1.33 to 1.47 MeV (where we omit here one of the early and imprecise results). This uncertainty is often larger than the provided errors of particular experiments. Even the most recent experiments [8,9], both of which have been declared to have the best precisions ever, disagree with each other for E_T values of the 0^+ state beyond the provided errors. Thus the overall experimental situation is unsatisfactory already for the 0^+ ^{16}Ne ground-state energies.

TABLE III. Experiments in which the properties of 0^+ g.s. and first 2^+ states in ^{16}Ne were measured. Energies and widths are in MeV. The last column provides the range of the ^{15}F g.s. energies $E_r(1/2^+)$ in which the consistency of theoretical TES values can be achieved for 0^+ and 2^+ states simultaneously (see Figs. 4 and 8).

Ref.	$E_T(0^+)$	$\Gamma(0^+)$	$E_T(2^+)$	$\Gamma(2^+)$	$E_r(1/2^+)$
[24]	1.33(8)	0.2(1)	3.02(11)		1.25–1.35
[25]	1.35(8)		3.2(2)	0.2(2)	1.27–1.4
[8]	1.388(15)	0.082(15)	3.220(46)	<0.05	none
[9]	1.466(20)	<0.08	3.16(2)	0.02(1)	1.39–1.42
[26]	1.8(5)				
[27]	1.466(45)				
[28]	1.399(24)	0.11(4)			

Among the experimental data given in Table III, the four experiments listed first [8,9,24,25] provide both the 0^+ and 2^+ positions and thus allow us to consider consistency of these data with theoretical TES results as was done for [9] in Fig. 4. Such a comparison is provided in Fig. 8. The consistency range for the experiment in Ref. [25], $E_r = 1.27$–1.4 MeV, is quite broad and somehow overlaps with that found for the data of Ref. [9]. Consistency in terms of the TES exists for the data from Ref. [24]. However, the obtained range of $E_r = 1.25$–1.35 MeV is not compatible with that of [9]. Finally, the results of [8] are not compatible in TES terms as calculated in our work (with the theoretical curves being crossed by the experimental ranges at somewhat different E_r ranges). It should be noted that if a larger uncertainty is assumed for the g.s. energy in this experiment, then consistency with theoretical results would be achieved at $E_r \sim 1.39$ MeV, also in agreement with [9].

We have demonstrated above in Figs. 5 and 6 that an increase in precision of the experimental data on the state positions is required to make better use of the TES results even for the most recent data of Ref. [9]. Figure 8 shows

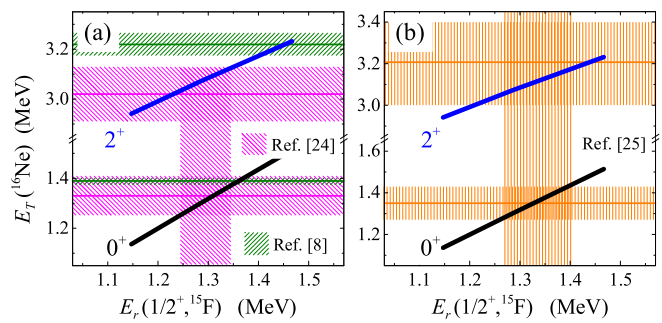

FIG. 8. (Color online) Dependence of the 0^+ and 2^+ state energies in ^{16}Ne on the position of the g.s. $1/2^+$ resonance in ^{15}F. The solid lines are the same as in Fig. 4. Horizontal gray lines and hatched areas show the experimental values from Refs. [8,24] (a) and Ref. [25] (b) with their uncertainties. The vertical hatched areas indicate the E_r ranges where consistency between theory and experiment is achieved.

that the overall situation is even worse and we see from the experimental side also a broad controversy concerning the older data, which should be resolved in general before definitive conclusions on actual TES behavior would become possible.

VI. THEORETICAL DISCUSSION

The obvious way to use the TES for nuclear structure studies in sd-shell systems with even number of valence nucleons is to apply it to the derivation of the configuration mixing rates. The basic idea was discussed in the Introduction related to Eq. (3). This way of reasoning about the nuclear structure was elaborated in a number of papers for various mirror pares of sd-shell systems: ^{12}O-^{12}Be [29], ^{15}Ne-^{15}B [30], ^{16}Ne-^{16}C [31,32], ^{17}Ne-^{17}N [33], and ^{18}Ne-^{18}O [31,34].

It is necessary to note that the connection between the TES and configuration mixing is straightforward and simple only in the case of an independent particle model with well-defined orbital characteristics. However, even in the independent particle model fixing of orbital sizes requires precise knowledge of excitation energies of the single-particle states for the $A-1$ "subsystem" on the proton side of the isobar. Among the mentioned systems this is not the case for ^{12}O, ^{15}Ne, and ^{16}Ne, with "subsystems" ^{11}N, ^{14}F, and ^{15}F which possess quite broad $s_{1/2}$ states making the precise experimental determination of CDE problematic. In this work we demonstrate by the example of ^{16}Ne that this issue has a major impact on conclusions about configuration mixing (see Fig. 6). On top of this issue we also insist on the existence of a dynamic three-body TES mechanism leading to a strong modification of configuration mixing rates when we move from the neutron to the proton side of the isobar.

Reference [30] provides an impressive prediction of the ^{15}Ne g.s. energy of $E_T = 2.68(24)$ MeV, which appears to be in a good agreement with the later measured value of $E_T = 2.522(66)$ MeV [8]. This prediction is based on two ingredients: (i) A phenomenological linear dependence on $W(s^2)$ for the "scaled CDE," $(S_{2n} - S_{2p})A^{1/3}/Z_<$, was derived in [30] based on the data for several $Z = 8$, 10 isobaric mirror partner pairs. (ii) A plausible value $W(s^2) = 66\%$ for ^{15}B was assumed in [30] just between the $W(s^2) = 86\%$ deduced for ^{14}Be and $W(s^2) = 46\%$ for ^{16}C. We point to the need to reconcile this type of phenomenology with more complicated dependencies obtained in this work. The dependence (i) is in principle analogous to the dependence of Fig. 5(a). However, we obtain a set of such dependencies even for one single nucleus ^{16}Ne depending on E_r in ^{15}F. Studies of configuration mixing in ^{15}Ne in a three-body model could also elucidate issue (ii).

VII. CONCLUSIONS

The following main results are obtained in this work.

(i) Large isospin symmetry breaking on the level of the nuclear structure associated with the TES was predicted in Ref. [4] for 0^+ states and further elaborated in this work also in the case of 2^+ states. We have found that in the ^{16}Ne-^{16}C mirror pair the "dynamic" component of the TES, connected to structure modification, is responsible for about half of the whole TES effect. The scale of the structure modification in these mirror nuclei is 20%–25% for the 0^+ ground states and 6%–10% for the first 2^+ states.

(ii) In this work we study carefully the stability of such predictions to theoretical inputs to the calculations. In our predictions the structure of the ^{16}Ne states appears to be very stable to the admissible variation of parameters. Quite unexpectedly, the stability of predictions for ^{16}Ne is much better than for ^{16}C, presumably due to a more peripheral character of its WF.

(iii) Accurate studies of the Coulomb displacement energies indicate that a consistency among three parameters should be needed: the decay energy E_T, the ^{15}F g.s. energy E_r, and the configuration mixing parameters $[W(s^2)/W(d^2)$ for 0^+ and $W(sd)/W(d^2)$ for 2^+ states]. This is a more complicated dependence than is ordinarily assumed. Typically the TES is correlated with configuration mixing *only* to provide predictions about nuclear structure [29–34].

(iv) The energy of the ^{15}F $1/2^+$ g.s. extracted from our analysis is $E_r = 1.39$–1.42 MeV. Some shift to lower energies is possible due to WF configurations which are beyond our model. The E_r values above 1.43–1.45 MeV are practically excluded by our analysis.

(v) The current experimental situation is too uncertain for high-precision comparison with the calculated results. Even the very accurate values of the ^{16}Ne experimental energies of Ref. [9] allow consistency with theoretical predictions of the TES in a broad range of other parameters. Further increase in the precision of the measured energies in ^{15}F and ^{16}Ne would impose very stringent limits on the parameter space in which consistency with theory is possible. Thus the TES could become a sensitive tool for extraction of deep structural information about ^{16}Ne-^{16}C mirror nuclei as well as sd-shell nuclei with analogous dynamics.

ACKNOWLEDGMENTS

L.V.G. is supported by Russian Foundation for Basic Research Grant No. 14-02-00090-a and Ministry of Education and Science of the Russian Federation Grant No. NSh-932.2014.2. We are grateful to Prof. J. S. Vaagen for careful reading of the manuscript and useful comments.

[1] R. G. Thomas, Phys. Rev. **88**, 1109 (1952).
[2] J. B. Ehrman, Phys. Rev. **81**, 412 (1951).
[3] N. Auerbach and N. Vinh Mau, Phys. Rev. C **63**, 017301 (2000).
[4] L. V. Grigorenko, I. G. Mukha, I. J. Thompson, and M. V. Zhukov, Phys. Rev. Lett. **88**, 042502 (2002).
[5] E. Garrido, D. V. Fedorov, and A. S. Jensen, Phys. Rev. C **69**, 024002 (2004).
[6] E. Comay, I. Kelson, and A. Zidon, Phys. Lett. B **210**, 31 (1988).
[7] I. Mukha *et al.*, Phys. Rev. C **77**, 061303 (2008).
[8] F. Wamers *et al.*, Phys. Rev. Lett. **112**, 132502 (2014).

[9] K. W. Brown *et al.*, Phys. Rev. Lett. **113**, 232501 (2014).
[10] B. V. Danilin, M. V. Zhukov, S. N. Ershov, F. A. Gareev, R. S. Kurmanov, J. S. Vaagen, and J. M. Bang, Phys. Rev. C **43**, 2835 (1991).
[11] M. Pfützner, M. Karny, L. V. Grigorenko, and K. Riisager, Rev. Mod. Phys. **84**, 567 (2012).
[12] L. V. Grigorenko, I. G. Mukha, and M. V. Zhukov, Nucl. Phys. A **713**, 372 (2003); Erratum Nucl. Phys. A **740**, 401 (2004).
[13] L. V. Grigorenko, Y. L. Parfenova, and M. V. Zhukov, Phys. Rev. C **71**, 051604 (2005).
[14] P. G. Sharov, I. A. Egorova, and L. V. Grigorenko, Phys. Rev. C **90**, 024610 (2014).
[15] A. Ozawa, T. Suzuki, and I. Tanihata, Nucl. Phys. A **693**, 32 (2001).
[16] D. Gogny, P. Pires, and R. D. Tourreil, Phys. Lett. B **32**, 591 (1970).
[17] L. V. Grigorenko *et al.*, Phys. Rev. C **80**, 034602 (2009).
[18] I. Angeli and K. Marinova, At. Data Nucl. Data Tables **99**, 69 (2013).
[19] H. T. Fortune, Phys. Rev. C **74**, 054310 (2006).
[20] W. A. Peters *et al.*, Phys. Rev. C **68**, 034607 (2003).
[21] V. Z. Goldberg, G. G. Chubarian, G. Tabacaru, L. Trache, R. E. Tribble, A. Aprahamian, G. V. Rogachev, B. B. Skorodumov, and X. D. Tang, Phys. Rev. C **69**, 031302 (2004).
[22] F. Q. Guo *et al.*, Phys. Rev. C **72**, 034312 (2005).
[23] I. Stefan *et al.*, Phys. Rev. C **90**, 014307 (2014).
[24] G. J. KeKelis, M. S. Zisman, D. K. Scott, R. Jahn, D. J. Vieira, J. Cerny, and F. Ajzenberg-Selove, Phys. Rev. C **17**, 1929 (1978).
[25] I. Mukha *et al.*, Phys. Rev. C **79**, 061301 (2009).
[26] R. Holt *et al.*, Phys. Lett. B **69**, 55 (1977).
[27] G. R. Burleson *et al.*, Phys. Rev. C **22**, 1180 (1980).
[28] C. J. Woodward, R. E. Tribble, and D. M. Tanner, Phys. Rev. C **27**, 27 (1983).
[29] R. Sherr and H. T. Fortune, Phys. Rev. C **60**, 064323 (1999).
[30] H. Fortune, Phys. Lett. B **718**, 1342 (2013).
[31] K. Ogawa, H. Nakada, S. Hino, and R. Motegi, Phys. Lett. B **464**, 157 (1999).
[32] H. T. Fortune and R. Sherr, Phys. Rev. C **66**, 017301 (2002).
[33] H. Fortune and R. Sherr, Phys. Lett. B **503**, 70 (2001).
[34] R. Sherr and H. T. Fortune, Phys. Rev. C **58**, 3292 (1998).